Tensor Train Subspace Analysis for Classification of Hand Gestures with Surface EMG Signals

Rafał Zdunek[0000−0003−3323−6717]

Faculty of Electronics, Photonics and Microsystems
Wroclaw University of Science and Technology
Wybrzeze Wyspianskiego 27, 50-370 Wroclaw, Poland
rafal.zdunek@pwr.edu.pl

Abstract. Processing and classification of surface EMG signals is a challenging computational problem that has received increasing attention for at least two decades. When multichannel EMG signals are transformed into spectrograms, classification can be performed using multilinear features that can be extracted from a set of spectrograms by various tensor decomposition methods. In this study, we propose to use one of the most efficient tensor network models, i.e. the tensor train decomposition method and to combine it with the tensor subspace analysis to extract the more discriminant 2D features from multi-way data. Numerical experiments, carried out on surface EMG signals registered during hand gesture actions, demonstrated that the proposed feature extraction method outperforms well-known tensor decomposition methods in terms of classification accuracy.

Keywords: Tensor train decomposition · Tensor subspace analysis · sEMG signal classification · hand gesture recognition

1 Introduction

Hand gestures are a form of non-verbal communication that is typically used by deaf-mute people but can also be used for human–computer interaction (HCI) through multiple mediums, such as vision, audition, tactition, etc. Surface electromyography (sEMG) is a technique for measuring the electrical activity produced by the skeletal muscles. The sEMG signals are associated with the movements of the healthy hand and fingers, and they can clearly represent the will of the user to control various devices, including computer desktops, hand prosthesis, exoskeletons, etc. Such signals can also contain meaningful information on static and dynamic hand gestures. Regarding this possibility, many sEMG-based HCI systems have been designed; see, e.g. [4, 14, 15].

Classification of sEMG signals is a challenging computational problem, mainly due to many sources of disturbance, such as motion artifacts, electrocardiographic artifacts, crosstalk, ambient noise, and inherent measurement device noise, which results in highly noisy observations, where the desired signal may be deeply hidden in the observations. Hence, raw sEMG must be adequately processed to extract the most relevant features for classification.

ICCS Camera Ready Version 2023
To cite this paper please use the final published version:
DOI: 10.1007/978-3-031-36021-3_63

In this study, we propose a new computational method to extract relevant features from sEMG signals that contain information on hand gestures. We used sEMG signals coming from the forearm and acquired in the dynamic gaming environment presented in [13]. Sliding a window in the time domain, and applying the short-time Fourier transform (STFT) to each signal in the slide, we get a set of spectrograms that can be collected in the form of a multiway array, referred to as an input tensor. The modes of the tensor represent the frequency, time, channel, and ordering of samples. Due to this representation, multi-modal features can be next extracted using various tensor decomposition methods. This concept was developed in [17], where several well-known matrix and tensor decomposition methods were compared for sEMG data collected from subjects performing various grasping movements. This study is based on the similar methodology, but we present here a new approach to multilinear feature extraction that is based on the tensor train (TT) decomposition method, additionally enhanced by the information on the geometry of observed samples. Moreover, the experiments are performed on different sEMG signals.

The remainder of this paper is organized as follows. In Section 2, we briefly discuss the related works. Section 3 presents the proposed method, preceded by the fundamentals of the TT model. The experimental results are described in Section 4. Finally, the conclusions are drawn in Section 5.

2 Related works

There are three basic approaches to extract features from sEMG signals that are outlined in the following domains: time, frequency, or time-frequency. Time-domain features, such as mean absolute value (MAV), slope sign changes (SSC), waveform lengths (WL), and zero crossings (ZC) [8], are useful for real-time processing and offer increased classification accuracy with respect to raw data. However, the analysis of strongly perturbed and nonstationary weak signals in the time domain is certainly not so efficient as in the time-frequency domain. There are many computational approaches for extracting time-varying frequency features from sEMG signals, in particular the continuous wavelet transform (CWT) that leads to scalograms and STFT that leads to spectrograms. In this study, we used SIFT because it is more suitable for processing nonstationary and highly noisy signals. Reviews of feature extraction methods for the classification of sEMG can be found in [1, 9, 16].

The TT model, known as the matrix product state (MPS) in quantum physics [12] and quantum chemistry [10], has gained a great popularity in the area of computational sciences, machine learning, and signal processing [2, 3]. However, to our best knowledge, it has never been used for feature extraction from sEMG signals. The TT undoubtedly combines multiple advantages that are important for our purpose. Therefore, the motivations behind the use of this model in our study can be stated as follows. First, it provides 2D features that capture multilinear information from all modes, which is more useful for classification than single 1D representations. Second, it is a multi-rank procedure

ICCS Camera Ready Version 2023
To cite this paper please use the final published version:
DOI: 10.1007/978-3-031-36021-3_63

that is more efficient than the standard CP decomposition but its computational and storage complexities are lower than for the standard Tucker decomposition. Third, its multimodal structure fits very well for augmented data. The last and probably the most important for this study, the TT model can be easily combined with the tensor subspace analysis (TSA) method [6], which is very profitable for classification tasks.

3 Methods

Notation: Multi-way arrays, matrices, vectors, and scalars are denoted by calligraphic uppercase letters (e.g., $\mathcal{Y}$), boldface uppercase letters (e.g., $\boldsymbol{Y}$), lowercase boldface letters (e.g., $\boldsymbol{y}$) and unbolded letters (e.g., y), respectively. Multi-way arrays will also be equivalently referred to as tensors [11],

3.1 Tensor train model

Let $\mathcal{Y} \in \mathbb{R}^{I_1 \times I_2 \times \ldots \times I_N}$ be the N-way array that is referred to as the N-th order tensor. The TT decomposition of $\mathcal{Y}$ can be expressed by the following model:

$$\mathcal{Y} = \sum_{r_1=1}^{R_1} \sum_{r_2=1}^{R_2} \ldots \sum_{r_{N-1}=1}^{R_{N-1}} \mathcal{Y}_1(1, :, r_1) \circ \mathcal{Y}_2(r_1, :, r_2) \circ \ldots \circ \mathcal{Y}_N(r_{N-1}, :, 1) \quad (1)$$

where $\forall n : \mathcal{Y}_n \in \mathbb{R}^{R_{n-1} \times I_n \times R_n}$ is the n-th core tensor, and symbol $\circ$ stands for the outer product. Set $\{R_0, R_1, \ldots, R_{N-1}, R_N\}$ determine the TT-ranks, where $R_0 = R_N = 1$. Cores $\mathcal{Y}_1 \in \mathbb{R}^{I_1 \times R_1}$ and $\mathcal{Y}_N \in \mathbb{R}^{R_{N-1} \times I_N}$ are the boundary matrices. Core tensors capture mode-related features, where $\mathcal{Y}_n$ contains the features related to the n-th mode of $\mathcal{Y}$.

Assuming $I_1 = \ldots = I_N = I$ and $R_1 = \ldots = R_N = R$, the storage complexities of the CANDECOM/PARAFAC (CP), Tucker, and TT decomposition models can be approximated by $\mathcal{O}(NIR)$, $\mathcal{O}(NIR + R^N)$, and $\mathcal{O}(NIR^2)$.

3.2 Proposed method

Let $\mathcal{Y} = [y_{i_1,\ldots,i_N}] \in \mathbb{R}^{I_1 \times \ldots \times I_N}$ be the N-th order tensor of observed samples ordered along the n-th mode, where $1 < n < N$. If the samples are ordered along the first or last mode, then $\mathcal{Y}$ should be permuted accordingly. We assume that $n = [N/2]$, where $[\cdot]$ rounds to the nearest integer number. Furthermore, due to the computational complexity of the TT decomposition, the first and last modes should contain the largest numbers of entries with respect to the other modes; expect the mode of ordering the samples.

Note that the TT model in (1) can be equivalently expressed in the element-wise notation:

$$y_{i_1,\ldots,i_N} = \boldsymbol{y}_1(i_1)^T \boldsymbol{Y}_2(i_2) \cdots \boldsymbol{Y}_{N-1}(i_{N-1}) \boldsymbol{y}_N(i_N), \quad (2)$$

ICCS Camera Ready Version 2023
To cite this paper please use the final published version:
DOI: 10.1007/978-3-031-36021-3_63

where $\boldsymbol{y}_1(i_1) = \mathcal{Y}_1(1, i_1, :) \in \mathbb{R}^{R_1}$ and $\boldsymbol{y}_N(i_N) = \mathcal{Y}_N(:, i_N, 1) \in \mathbb{R}^{R_N}$ are the i_1-th row of $\mathcal{Y}_1$ and i_N-th column of $\mathcal{Y}_N$, respectively, and $\boldsymbol{Y}_n(i_n) \in \mathbb{R}^{R_{n-1} \times R_n}$ are lateral slices of core tensor $\mathcal{Y}_n$ for $i_n = 1, \ldots, I_n$ and $n = 2, \ldots, N-1$.

A tensor train subspace is determined by cores $\{\mathcal{Y}_1, \ldots, \mathcal{Y}_N\}$ and is invariant with respect to the orthogonal transformations between modes. However, we slightly alleviate this condition by taking the following approximations:

$$\begin{aligned} y_{i_1,\ldots,i_N} &= \boldsymbol{y}_{(\leq n-1)}^T \boldsymbol{Y}_n(i_n) \boldsymbol{y}_{(\geq n+1)} = \boldsymbol{y}_{(\leq n-1)}^T \boldsymbol{U}\boldsymbol{U}^T \boldsymbol{Y}_n(i_n) \boldsymbol{V}\boldsymbol{V}^T \boldsymbol{y}_{(\geq n+1)} \\ &\cong \boldsymbol{y}_{(\leq n-1)}^T \tilde{\boldsymbol{U}} \left(\tilde{\boldsymbol{U}}^T \boldsymbol{Y}_n(i_n) \tilde{\boldsymbol{V}} \right) \tilde{\boldsymbol{V}}^T \boldsymbol{y}_{(\geq n+1)} \\ &= \tilde{\boldsymbol{y}}_{(\leq n-1)}^T \tilde{\boldsymbol{Y}}_n(i_n) \tilde{\boldsymbol{y}}_{(\geq n+1)}, \end{aligned} \tag{3}$$

where $\boldsymbol{y}_{(\leq n-1)} = \boldsymbol{y}_1(i_1)^T \boldsymbol{Y}_2(i_2) \cdots \boldsymbol{Y}_{n-1}(i_{n-1}) \in \mathbb{R}^{R_{n-1}}$ aggregates the features from the first to the $(n-1)$-th mode, and the features from the $(n+1)$-th mode to the last are represented by $\boldsymbol{y}_{(\geq n+1)} = \boldsymbol{Y}_{n+1}(i_{n+1}) \cdots \boldsymbol{Y}_{N-1}(i_{N-1}) \boldsymbol{y}_N(i_N) \in \mathbb{R}^{R_n}$. Matrices $\boldsymbol{U} \in \mathbb{R}^{R_{n-1} \times R_{n-1}}$ and $\boldsymbol{V} \in \mathbb{R}^{R_n \times R_n}$ are orthogonal matrices, i.e. $\boldsymbol{U}\boldsymbol{U}^T = \boldsymbol{I}_{R_{n-1}}$ and $\boldsymbol{V}\boldsymbol{V}^T = \boldsymbol{I}_{R_n}$. Projection matrices $\tilde{\boldsymbol{U}} \in \mathbb{R}^{R_{n-1} \times J_1}$ and $\tilde{\boldsymbol{V}} \in \mathbb{R}^{R_n \times J_2}$ are created from $\boldsymbol{U}$ and $\boldsymbol{V}$ by selecting the columns that correspond to the most significant eigenvalues, where $J_1 < R_{n-1}$ and $J_2 < R_n$. Thus, $\tilde{\boldsymbol{Y}}_n(i_n) \in \mathbb{R}^{J_1 \times J_2}$ contains the features of $\boldsymbol{Y}_n(i_n)$ projected onto the bases spanned by $\tilde{\boldsymbol{U}}$ and $\tilde{\boldsymbol{V}}$.

To calculate the projection matrices, the concept of the TSA method [6] can be applied, which leads to the following optimization problem:

$$\min_{\tilde{\mathbf{U}}, \tilde{\mathbf{V}}} \frac{1}{2} \sum_{i_n^{(1)}=1}^{I_n} \sum_{i_n^{(2)}=1}^{I_n} s_{i_n^{(1)}, i_n^{(2)}} ||\tilde{\boldsymbol{Y}}_n(i_n^{(1)}) - \tilde{\boldsymbol{Y}}_n(i_n^{(2)})||_F^2, \tag{4}$$

where $\boldsymbol{S} = [s_{i_n^{(1)}, i_n^{(2)}}] \in \mathbb{R}^{I_n \times I_n}$ is the weight matrix that can be expressed by the heat kernel:

$$s_{i_n^{(1)}, i_n^{(2)}} = \begin{cases} \exp\left\{ -\dfrac{||\mathcal{Y}(i_n^{(1)}) - \mathcal{Y}(i_n^{(2)})||_F^2}{\tau} \right\}, & \text{if } \mathcal{Y}(i_n^{(1)}) \text{ and } \mathcal{Y}(i_n^{(2)}) \\ & \text{belong to the same class} \\ 0 & \text{otherwise} \end{cases}. \tag{5}$$

for $\tau > 0$. Samples $\left\{ \mathcal{Y}(i_n^{(1)}), \mathcal{Y}(i_n^{(2)}) \right\} \in \mathbb{R}^{I_1 \times \ldots \times I_{n-1} \times I_{n+1} \times \ldots \times I_N}$ form $\mathcal{Y} = \texttt{cat}\{\mathcal{Y}(i_n = 1), \ldots, \mathcal{Y}(i_n = I_n), 1\}$ for $i_n^{(1)}, i_n^{(2)} \in \{1, \ldots, I_n\}$.

Following straightforward computations, the objective function in (4) takes the form:

$$\Psi = \text{tr}\{\tilde{\boldsymbol{V}}^T \boldsymbol{D}_V \tilde{\boldsymbol{V}}\} - \text{tr}\{\tilde{\boldsymbol{V}}^T \boldsymbol{S}_V \tilde{\boldsymbol{V}}\}, \tag{6}$$

where

$$\boldsymbol{D}_V = \sum_{i_n^{(1)}=1}^{I_n} d_{i_n^{(1)}} \boldsymbol{Y}_n(i_n^{(1)})^T \tilde{\boldsymbol{U}}\tilde{\boldsymbol{U}}^T \boldsymbol{Y}_n(i_n^{(1)}) \in \mathbb{R}^{R_n \times R_n} \tag{7}$$

ICCS Camera Ready Version 2023
To cite this paper please use the final published version:
DOI: 10.1007/978-3-031-36021-3_63

with $d_{i_n^{(1)}} = \sum_{i_n^{(2)}=1}^{I_n} s_{i_n^{(1)},i_n^{(2)}}$,

$$\boldsymbol{S}_V = \sum_{i_n^{(1)}=1}^{I_n} \sum_{i_n^{(2)}=1}^{I_n} s_{i_n^{(1)},i_n^{(2)}} \boldsymbol{Y}_n(i_n^{(1)})^T \tilde{\boldsymbol{U}} \tilde{\boldsymbol{U}}^T \boldsymbol{Y}_n(i_n^{(2)}) \in \mathbb{R}^{R_n \times R_n}. \tag{8}$$

According to the assumptions of the spectral graph theory and locality preserving projections (LPP) [7], problem (4) with respect to $\tilde{\boldsymbol{V}}$ can be reformulated in terms of the generalized Rayleigh quotient:

$$\max_{\tilde{\mathbf{V}}} \frac{\mathrm{tr}\{\tilde{\boldsymbol{V}}^T \left(\boldsymbol{S}_V - \boldsymbol{D}_V\right) \tilde{\boldsymbol{V}}\}}{\mathrm{tr}\{\tilde{\boldsymbol{V}}^T \boldsymbol{D}_V \tilde{\boldsymbol{V}}\}}. \tag{9}$$

The solution to (9) can be approximated by computing generalized eigenvectors that are associated with the J_2 most significant eigenvalues of the pair of matrices $\{\left(\boldsymbol{D}_V - \boldsymbol{S}_V\right), \boldsymbol{D}_V\}$.

Similarly, the solution to (4) with respect to $\tilde{\boldsymbol{U}}$ can be found following a similar computational strategy. The computations of both factors require the use of an alternating optimization procedure.

To obtain core tensors $\{\mathcal{Y}_1, \ldots, \mathcal{Y}_N\}$ from the training samples in $\mathcal{Y}$, we used the both-side recursive update algorithm (Algorithm 1) from [5]. A similar approach was used to compute the projection of the testing samples onto the tensor space spanned by the training factors (Algorithm 2 in [5]). The proposed procedure for extracting 2D features is summarized in Algorithm 1.

Algorithm 1 TSA-TT feature extraction

Input : $\mathcal{Y} \in \mathbb{R}^{I_1 \times \ldots \times I_N}$ – N-way array of multilinear training samples collected along the n-th mode ($1 < n < N$), $\mathcal{Y}^{(test)} \in \mathbb{R}^{I_1 \times \ldots \times I_{n-1} \times I_K \times I_{n+1} \times \ldots \times I_N}$ – N-way array of I_K multilinear testing samples, $\boldsymbol{J} = [J_1, \ldots, J_{N-1}]$ – TT-ranks, (J_1, J_2) – TSA ranks

Output: $\mathcal{Z} \in \mathbb{R}^{I_n \times J_1 \times J_2}$ – estimated 2D training features, $\mathcal{Z}^{(test)} \in \mathbb{R}^{I_K \times J_1 \times J_2}$ – estimated 2D testing features

Compute weight matrix $\boldsymbol{S}$ according to (5),
Compute $[\mathcal{Y}_1, \ldots, \mathcal{Y}_N] = \texttt{TT} - \texttt{SVD}(\mathcal{Y}, \boldsymbol{J})$; `// Algorithm 1 from [5]`
Compute $\tilde{\boldsymbol{U}}$ and $\tilde{\boldsymbol{V}}$ by solving problem (4),
Run projection: $\mathcal{Z}(i_n, :, :) = \tilde{\boldsymbol{U}}^T \mathcal{Y}_n(i_n) \tilde{\boldsymbol{V}} \in \mathbb{R}^{J_1 \times J_2}$ for $i_n = 1, \ldots, I_n$,
Compute $[\mathcal{Y}_n^{(test)}] = \texttt{Tensorproj}(\mathcal{Y}^{(test)}, \mathcal{Y}_1, \ldots, \mathcal{Y}_N)$; `// Algorithm 2 from [5]`
Run projection: $\mathcal{Z}^{(test)}(i_k, :, :) = \tilde{\boldsymbol{U}}^T \mathcal{Y}_n(i_k)^{(test)} \tilde{\boldsymbol{V}} \in \mathbb{R}^{J_1 \times J_2}$ for $i_k = 1, \ldots, I_K$,

Remark 1. Assuming $J = J_1 = J_2$, the computational complexity of the TSA methods can be roughly estimated as $\mathcal{O}\left(4KIR_{n-1}R_nI_n^2\right)$, where K is the number of alternating iterations. The TT core tensors in the `TT-SVD` algorithm can be

ICCS Camera Ready Version 2023
To cite this paper please use the final published version:
DOI: 10.1007/978-3-031-36021-3_63

computed with $\mathcal{O}(\sum_{n=1}^{N}\prod_{r=1}^{n}R_r\prod_{p=n}^{N}I_p)$. Therefore, if the number of training samples is large, TSA may predominate in the overall computational complexity. However, I_n is rather a small number in the application discussed.

4 Results and Discussion

Experiments were conducted on publicly available sEMG signals [13] from the UCI Machine Learning Repository [1]. The 8 channel sEMG signals were collected from 36 healthy subjects, aged 18 to 47 years, during PC gaming activity. The MYO Thalmic bracelet was equipped with 8 sensors equally spaced around the forearm. The subjects performed the following hand gestures: 1 – hand clenched in a fist, 2 – wrist flexion, 3 – wrist extension, 4 – radial deviations, 5 – ulnar deviations, 6 – extended palm. Two series of experiments are carried out, and each gesture lasts for 3 seconds.

The temporal signals from each channel were converted into spectrograms using the Matlab `spectrogram` function with the parameters: window length – 64 samples, overlapping – 54 samples, frequency sampling points – 256. The spectrograms were then partitioned into non-overlapping blocks of 64 samples with respect to the time axis. The blocks in which the signal energy was below a given threshold were neglected. Other blocks were processed with local averaging 2D filtration in the log scale, and then ordered in the form of 4-way array $\mathcal{Y} \in \mathbb{R}^{129\times 64\times 8\times 36}$, where the successive modes correspond to the frequency bins, the temporal resolution, the channels, and the number of labeled samples. The data were divided into the training and testing sets according to the 4-fold cross-validation (CV) rule.

The following algorithms were compared: HO-SVD (Higher-order singular value decomposition) [17], HALS-NTF (Hierarchical alternating least squares nonnegative tensor factorization) [3], SVD-TT (Tensor train based on singular value decomposition) [5], TT-SVD-TSA (proposed method). Negative input entries for HALS-NTF were replaced with the zero value. Due to the nonconvexity issue of the HALS-NTF, and the randomness of the CV splitting, the Monte Carlo (MC) analysis was carried out with 20 runs for each algorithm.

The Hinton diagrams of the confusion matrices obtained with the algorithms tested in the first series with the first subject are illustrated in Fig. 1. The average accuracy is given in parentheses in the caption of the figure. The elapsed time of the algorithms tested for both series with the first subject is depicted in Fig. 2(a). The range of the standard deviation is marked with the whiskers. The average accuracy obtained with TSA-TT in both series and with all the subjects is presented in Fig. 2(b).

5 Conclusions

The results presented in Fig. 1 demonstrate that TT-based methods lead to higher classification accuracy of sEMG signals than standard tensor factorization

[1] https://archive.ics.uci.edu/ml/datasets/EMG+data+for+gestures

ICCS Camera Ready Version 2023
To cite this paper please use the final published version:
DOI: 10.1007/978-3-031-36021-3_63

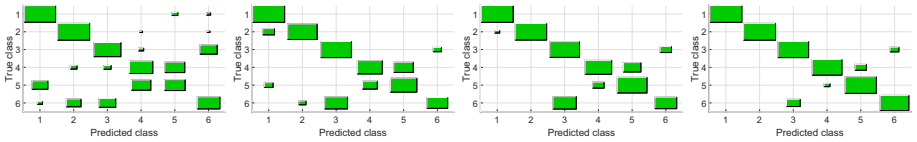

Fig. 1. Hinton diagrams of the confusion matrices obtained with the algorithms: (a) HO-SVD (Acc = 66.11 %), (b) HALS-NTF (Acc = 75 %), (c) SVD-TT (Acc = 80.97 %), (d) TSA-TT (Acc = 92.5 %). The accuracy is given in parentheses.

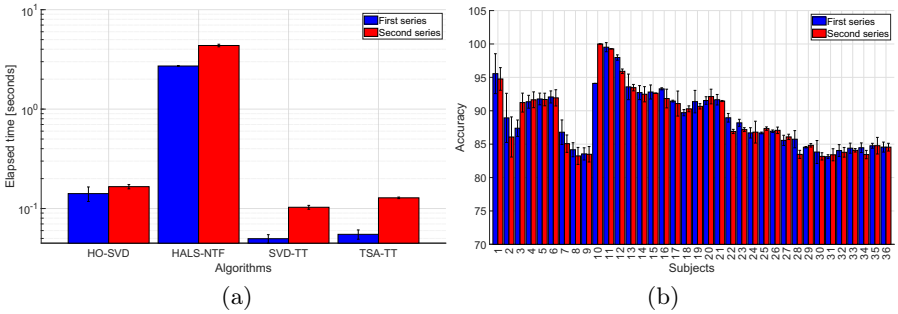

Fig. 2. (a) Elapsed time (in seconds) for all the methods in both series with the first subject, (b) accuracy of TSA-TT for all subjects and both series.

models, such as HO-SVD and HALS-NTF. Furthermore, the proposed method (TSA-TT) outperforms all the tested methods. The most challenging task is to classify an extended palm, especially with HO-SVD, but this is not a problem for TSA-TT. The efficiency of TSA-TT results from two aspects: first, due to the use of the TT model which better captures multilinear relationships, and second, it results from the incorporation of discriminant information on the geometry of training samples. Interestingly, the use of TSA did not affect the computational complexity considerably, as shown in Fig. 2(a). Among the algorithms tested, only HALS-NTF is substantially slower. The proposed method was also used in both series of experiments with all the subjects (see Fig. 2(b)). The results show that the accuracy of classification depends quite strongly on the subject. More research is needed to explain this phenomenon.

In summary, the proposed method significantly outperforms the other tested methods in terms of classification accuracy and has potential for applications in other classification problems. In future research, it can be used in various remote control systems, e.g. in desktop or hand prosthesis control.

ICCS Camera Ready Version 2023
To cite this paper please use the final published version:
DOI: 10.1007/978-3-031-36021-3_63

References

1. Chowdhury, R.H., Reaz, M.B.I., Ali, M.A.B.M., Bakar, A.A.A., Chellappan, K., Chang, T.G.: Surface electromyography signal processing and classification techniques. Sensors **13**(9), 12431–12466 (2013)
2. Cichocki, A., Lee, N., Oseledets, I.V., Phan, A.H., Zhao, Q., Mandic, D.P.: Tensor networks for dimensionality reduction and large-scale optimization: Part 1 low-rank tensor decompositions. Foundations and Trends in Machine Learning **9**(4-5), 249–429 (2016)
3. Cichocki, A., Phan, A.H., Zhao, Q., Lee, N., Oseledets, I.V., Sugiyama, M., Mandic, D.P.: Tensor networks for dimensionality reduction and large-scale optimization: Part 2 applications and future perspectives. Foundations and Trends in Machine Learning **9**(6), 431–673 (2017)
4. Côté-Allard, U., Fall, C.L., Drouin, A., Campeau-Lecours, A., Gosselin, C., Glette, K., Laviolette, F., Gosselin, B.: Deep learning for electromyographic hand gesture signal classification using transfer learning. IEEE Transactions on Neural Systems and Rehabilitation Engineering **27**(4), 760–771 (2019)
5. Fonał, K., Zdunek, R.: Distributed and randomized tensor train decomposition for feature extraction. In: IJCNN. pp. 1–8 (2019)
6. He, X., Cai, D., Niyogi, P.: Tensor subspace analysis. In: Weiss, Y., Schölkopf, B., Platt, J. (eds.) Advances in Neural Information Processing Systems. vol. 18. MIT Press (2005)
7. He, X., Niyogi, P.: Locality preserving projections. In: In Advances in Neural Information Processing Systems 16. MIT Press (2003)
8. Hudgins, B., Parker, P.A., Scott, R.N.: A new strategy for multifunction myoelectric control. IEEE Transactions on Biomedical Engineering **40**, 82–94 (1993)
9. Inam, S., Harmain, S.A., Shafique, S., Afzal, M., Rabail, A., Amin, F., Waqar, M.: A brief review of strategies used for emg signal classification. In: 2021 International Conference on Artificial Intelligence (ICAI). pp. 140–145 (2021)
10. Khoromskaia, V., Khoromskij, B.N.: Tensor numerical methods in quantum chemistry: from hartreefock to excitation energies. Phys. Chem. Chem. Phys. **17**, 31491–31509 (2015)
11. Kolda, T.G., Bader, B.W.: Tensor decompositions and applications. SIAM Review **51**(3), 455–500 (2009)
12. Lanyon, B.P., Maier, C., Holzäpfel, M., Baumgratz, T., Hempel, C., Jurcevic, P., Dhand, I., Buyskikh, A.S., Daley, A.J., Cramer, M., Plenio, M.B., Blatt, R., Roos, C.F.: Efficient tomography of a quantum many-body system. Nature Physics **13**, 1158?1162 (July 2017)
13. Lobov, S., Krilova, N., Kastalskiy, I., Kazantsev, V., Makarov, V.A.: Latent factors limiting the performance of semg-interfaces. Sensors **18**(4) (2018)
14. Ozdemir, M.A., Kisa, D.H., Guren, O., Akan, A.: Hand gesture classification using time–frequency images and transfer learning based on cnn. Biomedical Signal Processing and Control **77**, 103787 (2022)
15. Qi, J., Jiang, G., Li, G., Sun, Y., Tao, B.: Intelligent human-computer interaction based on surface EMG gesture recognition. IEEE Access **7**, 61378–61387 (2019)
16. Sultana, A., Ahmed, F., Alam, M.S.: A systematic review on surface electromyography-based classification system for identifying hand and finger movements. Healthcare Analytics **3**, 100126 (2023)
17. Wołczowski, A., Zdunek, R.: Electromyography and mechanomyography signal recognition: Experimental analysis using multi-way array decomposition methods. Biocybernetics and Biomedical Engineering **37**(1), 103–113 (2017)

ICCS Camera Ready Version 2023
To cite this paper please use the final published version:
DOI: 10.1007/978-3-031-36021-3_63